Computational / Experimental Study of a Variable Critical Nozzle Flow

Jae-Hyung Kim, Heuy-Dong Kim
(Andong University, Andong, Korea)
Kyung-Am Park
(Korea Research Institute of Standards and Science, Daejon, Korea)

Abstract Recently, critical nozzles have been extensively utilized to measure the mass flow rate in a variety of industrial applications. For the measurement of the mass flow rates at a wide range of operation conditions, the critical nozzle is required to be designed with different diameters. The objective of the present study is to investigate the effectiveness of a variable critical nozzle. A rod with a small diameter is inserted into the critical nozzle to change the effective cross-sectional area of the critical nozzle. Experimental work is performed to measure the mass flow rate of the critical nozzle with rod. Computational work is carried out using the 2-dimensional, axisymmetric, compressible Navier-Stokes equations which are discretized using a fully implicit finite volume method. The diameter of the rod is varied to obtain different mass flow rates through the variable critical nozzle. Computational results predict well the measured mass flow rates. The boundary layer displacement and momentum thickness at the throat of the critical nozzle are given as a function of Reynolds number. The discharge coefficient of the critical nozzle is given as an empirical equation.

Keywords: Compressible Flow, Flow Choke, Variable Critical Nozzle, Boundary Layer, Discharge Coefficient, Internal Flow

1. Introduction

In compressible gas flows with a sufficiently high pressure ratio, the flow is choked at a minimum cross-sectional area of flow passage, in which the mass flow rate reaches a maximum value. In this case, the mass flow is determined only by the stagnation conditions upstream of the flow passage[1].

For instance, compressible gas flow through a convergent-divergent nozzle is choked at the nozzle throat under a certain critical pressure ratio. For a pressure ratio larger than the critical pressure ratio, the mass flow does not change with the pressure ratio. According to one-dimensional gasdynamics theory, the mass flow rate is functions of the pressure and temperature at the upstream stagnation conditions, the diameter of nozzle throat and the ratio of specific heats of gas[2]. This phenomenon is one of unique features of the compressible internal flows.

In the past, much attention was paid on the prediction of mass flow through a flow passage, since it was of practical importance in a variety of industrial and engineering fields. The critical nozzle is used as a device to measure the mass flow with only the nozzle supply conditions. A lot of real picture has been learned from the flow rate measurements in highly elaborate experiment facilities[3,4].

According to these results, the mass flow rate and critical pressure ratio are a strong function of Reynolds number. Even over the critical pressure ratio, the mass flow rate was somewhat influenced by the radius of curvature of nozzle throat and angle of diffuser configuration[5,6], as well. This is due to viscous and heat transfer effects of gas flows through the critical nozzle. The total pressure losses occurring in the diffuser can play a role of the back pressure to the critical nozzle, consequently influencing the effective pressure ratio for the flow choking. In part,

3-dimensional effects and flow unsteadiness may be involved in predicting of the mass flow rate[7,8].

The previous works have shown that the discharge coefficient of the critical nozzle flow is a strong function of Reynolds number, based upon the velocity at the nozzle throat and the diameter of nozzle throat[9,10]. For high Reynolds numbers, the discharge coefficient approaches unity, indicating that the one-dimensional inviscid theory is valid for the prediction of the mass flow rate. It is, however, known that for lower Reynolds numbers, the discharge coefficient reduces considerably below unity[8,9]. This is due to the wall boundary layer effects on the mass flow rate through the critical nozzle.

Several experimental works have been done to investigate the discharge coefficient for low Reynolds numbers[11,12]. For a small critical nozzle, the Reynolds number can be low, and in this case, the prediction of the mass flow rate is not straightforward since it can be affected by the downstream pressure change even under the condition of the critical pressure ratio.

For the critical nozzle operating at a wide range of Reynolds numbers, the throat diameter of nozzle should be varied to measure the mass flow rate. A number of critical nozzles are needed to obtain different mass flow rates. This may be achieved by a variable critical nozzle, in which the throat diameter can be varied by means of a cost-effective simple method. A rod or a cone can be inserted into the critical nozzle to change the effective diameter at nozzle throat.

As a fundamental work to investigate a variable critical nozzle flow, the objective of the present study is to explore the effectiveness of a variable critical nozzle. A rod of a small diameter is inserted into the conventional critical nozzle so that the effective cross-sectional area at nozzle throat can be varied. Experimental work is performed to measure the mass flow rate through a variable critical nozzle. The axisymmetric, compressible, Navier-Stokes equations are solved using a finite volume method. The predicted results are validated using the experimental data.

2.Experimental apparatus and measurement

Experimental work has been carried out at Korea Research Institute of Standards and Science(KRISS). The experimental facility consists of compressor, storage tank, filter and dryer device, temperature control unit, test nozzle, bell prover system and timer. Compressed air passes through the double sets of filter and dryer systems, as schematically shown in Fig.1. Then the dew point of working gas is maintained at about $-40^{o}C$. At the temperature control unit, the temperature of working gas is very close to the room temperature. The temperature is measured using a platinum resistance thermometer ($100\,\Omega$, uncertainty

A pressure regulator locates upstream of the test nozzle to control the stagnation pressure of working gas, which is maintained constant during test. The stagnation pressure is measured using a pressure transducer, Ruska 6000 (pressure range 5MPa, uncertainty of $\pm 0.2\%$).

A back pressure regulator locates just downstream of the test nozzle. It can control the back pressure of the critical nozzle. In the present study, the back pressure is maintained constant at atmospheric pressure. The bell prover systems[13] directly measure the mass flow rate of the flow passing through the critical nozzle. These systems can measure the volume flow rate at maximum $10{,}000m^3/h$[9].

Detailed structure and operation of the bell prover system are reported in Ref(13). A cylinder of the prover is raised by gas flow through the critical nozzle. Then the height of cylinder is measured by laser interferometer. The collecting time of gas flow is measured by a timer using an optical sensor which is attached to the cylinder of the bell prover. To calculate the mass flow rate from the measured volume flow rate, the pressure and temperature inside the bell prover are measured. The present bell prover system for mass flow rate measurement has an uncertainty of $\pm 0.14\%$.

In the present study, the ratio of the back pressure to the upstream stagnation pressure is varied in the range between 253.3 and 557.3kPa. The tested Reynolds numbers are in the range between 87800 and 193300.

Thus, the flow through the critical nozzle can be considered to be typically turbulent.

Figure 2 shows the schematic of the variable critical nozzle, which is composed of a critical nozzle, a rod and a rod supporter. It has a diameter of $D(8.4639mm)$ at the nozzle throat, and the radius of curvature upstream of the nozzle throat is twice the throat diameter D. The critical nozzle has a diffuser with a half-angle(θ)of $4°$and a length of five times the throat diameter. The wall of the nozzle is polished so that the surface roughness effect can be negligible. A rod with a diameter of d is inserted into the critical nozzle in the axial direction. The effective diameter of the nozzle throat is varied depending on the diameter of the rod. In the present study, the diameter of the nozzle throat with a rod is calculated as an equivalent diameter D_{eq} which has the same cross-sectional area at nozzle throat. The rod is bolted to support it both upstream and downstream of the nozzle, and the rods with different diameters are inserted to change D_{eq}.

3. Computational method

The gas flow through critical nozzle is also simulated using a CFD method. The governing equations are given by the conservation forms of mass, momentum and energy. The axisymmetric, mass averaged, time-dependent Navier-Stokes equations are, in detail, described in Ref.(14). The governing equations are discretized spatially using a fully implicit finite volume scheme, in which the physical domain is subdivide into numerical cells and the integral equations are applied to each cell. An explicit multi-stage time stepping scheme, which is advanced from time t to time $t+\Delta t$ with a multi-stage Runge-Kutta scheme, is employed for the time derivatives involved in the governing equations.

The computational domain is extended up to the region of $6D$ upstream of the nozzle inlet and up to the region of $10D$ downstream of the nozzle exit. The boundary conditions are inlet total pressure and outlet static pressure, at the upstream and downstream boundaries, respectively. The the adiabatic, no-slip conditions are applied to the solid walls.

A structured grid system of about 40,000 grid points was employed in computations. The grids were densely clustered in boundary layers, so that those provided more reasonable predictions. In the present computations, the total pressure p_o and back pressure p_b are given at the inlet and outlet of the nozzle, respectively. The back pressure p_b is kept constant at 101.3kPa, but the inlet total pressure p_o is varied in the range below 5.5 p_b to change Reynolds number. Working gas is air and its temperature is kept constant at $T_o=300K$.

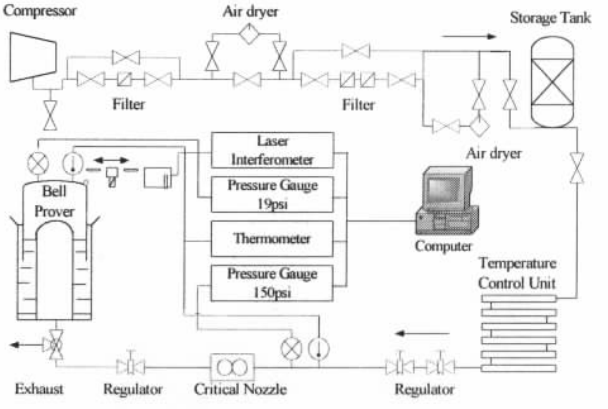

Fig.1 Schematic diagram of gas flow measurement electronics

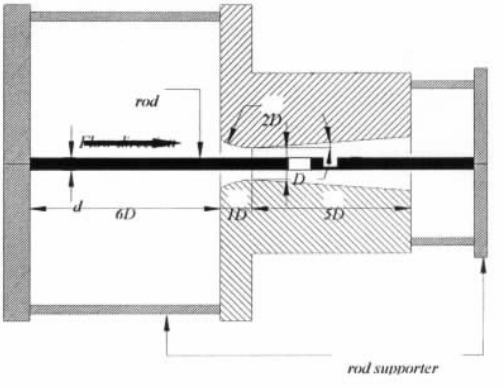

Fig.2 Schematic diagram of critical nozzle with rod

4. Results and discussion

In the present study, the total pressure at the nozzle inlet is varied to obtain different Reynolds number of the gas flow through the critical nozzle. The Reynolds number is given by,

$$\mathrm{Re} = \frac{4 \times \dot{m}_{theo}}{\pi \times D_{eq} \times \mu_o} \qquad (1)$$

where μ_o and $\dot{m}_{theo}$ are the coefficient of dynamic viscosity at the nozzle inlet conditions, and the theoretical mass flow rate, respectively. The characteristic length D_{eq} is the equivalent diameter of nozzle throat.

Figure 3 shows the computed static pressure distributions along the nozzle wall and the centerline of nozzle for four different Reynolds numbers, where x is the axial distance having an origin at the nozzle throat. The computed static pressure distributions are strongly dependent on Reynolds number, mainly at the region of $x/D>2.5$. The static pressure along the nozzle wall decreases monotonously with distance and it continues to decrease up to x/D of about 2.5. This means that the flow becomes supersonic downstream of the nozzle throat. Then the flow meets shock waves, leading to a sudden increase in the static pressure and the flow decelerates to subsonic speed. The shock wave moves downstream, as Reynolds number increases. The static pressure rise due to shock wave appears rather gradual. This is associated with the shock wave boundary layer interaction[15]. The static pressure rise seems to decrease as the shock wave moves.

Meanwhile, the static pressure distributions on the centerline of nozzle is quite similar to those along the nozzle wall, before the flow meets shock wave, but much steeper pressure rise is made through the shock wave. Just downstream of the shock wave, the flow is reaccelerated due to the post-shock expansion phenomenon[16], leading to a multiple of shock waves. The shock wave moves downstream as Reynolds number increases. It is noted that the static pressure rise on the centerline of nozzle is much steeper and greater, compared with that along the nozzle wall surface. This is due to the shock wave/boundary layer interaction on the wall surface.

A rod is inserted into the critical nozzle to make the same equivalent diameter as described in Fig.4. The computed static pressure distributions along the nozzle wall and the rod surface are presented in Fig.4. It is interesting to note that the static pressure rise due to shock wave moves further upstream, compared with the cases of the same Reynolds number as in Fig.3, and that the nozzle wall static pressure distributions are not significantly different from those on the rod surface. It is, thus, believed that inserting a rod into the critical nozzle makes the flow to be more uniform.

For a given value of $p_o / p_b = 2.5$, the equivalent diameter of the nozzle throat with a rod considerably influences the nozzle wall static pressure distributions, as shown in Fig. 5. Here it is noted that an increase in the diameter of rod reduces the equivalent diameter of the nozzle throat D_{eq}. The present computations show that the shock wave occurring downstream of the nozzle throat moves upstream, as D_{eq} increases. This is attributed to a change rate in the cross-sectional area by inserting the rod into the critical nozzle.

According to the previous studies[5,14], the discharge coefficient of the gas flow through a critical nozzle is given as a function of $1/(Re)^{1/2}$. From the present study, the correlation of the discharge coefficient is presented in Fig. 6. For the critical nozzle without rod, the present computations predict the experimental discharge coefficient in quite good accuracy, and in this case, an empirical equation is given by,

$$C_d = 0.9823 - 3.716 \times \frac{1}{\sqrt{\mathrm{Re}}} \qquad (2)$$

It seems that the discharge coefficient C_d of the critical nozzle with rod is dependent on D_{eq}, and leading to increasing C_d with D_{eq}. The present computations predict well the experimental discharge coefficient at comparatively high Reynolds numbers, but the prediction becomes somewhat poor in the range at low Reynolds numbers. Both the present experimental and computed results show that the discharge coefficient for the critical nozzle with rod is more sensitive to Reynolds number, compared with that of the cases without rod. Furthermore, the dependency of C_d on Reynolds number is more significant as D_{eq} decreases. This is due to the increased viscous effects with decreasing D_{eq}.

The present experimental and computed results show that the discharge coefficient of the critical nozzle with rod can be given as a function of Reynolds

number. Thus, Eq.(2) may be also yielded in the critical nozzle with rod after some corrections, as follows;

$$C_d = (0.9823 + a) - (3.716 + b) \times \frac{1}{\sqrt{\mathrm{Re}}} \qquad (3)$$

where a and b are the correction coefficients which can be related to the perimeter at the nozzle throat. Figure 7 presents the correction coefficients as a function of the perimeter w at the throat of the critical nozzle with rod, where two curves related to a and b are given by

$$a = 0.01187 \times \ln(w/D) + 0.1154 \qquad (4)$$
$$b = 13.8120 \times \ln(w/D) + 125.59 \qquad (5)$$

In Fig. 7, both a and b are functions of increasing w/D.

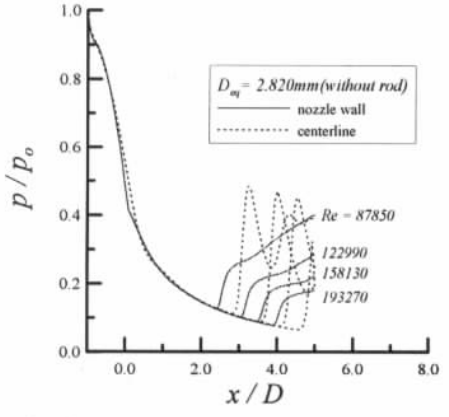

Fig.3 Predicted static pressure distributions along the nozzle wall and centerline

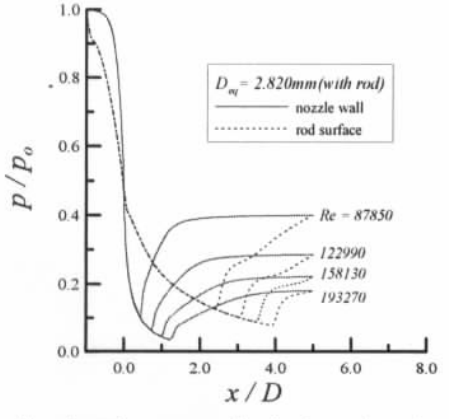

Fig.4 Predicted static pressure distributions along the nozzle wall and rod surface

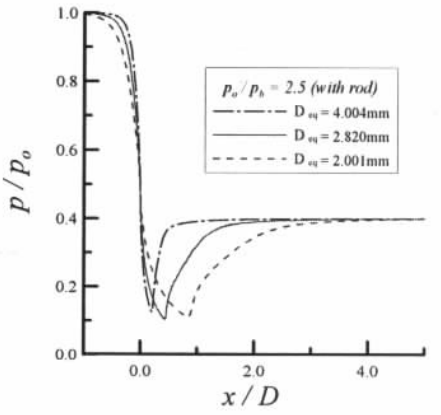

Fig.5 Effect of the rod diameter on the static pressure distribution along the nozzle wall ($p_o / p_b = 2.5$)

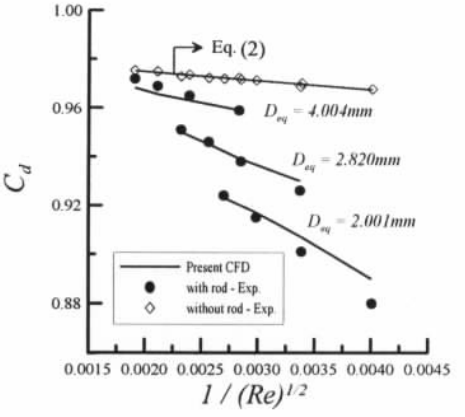

Fig.6 Variation of discharge coefficient (C_d) with Reynolds number

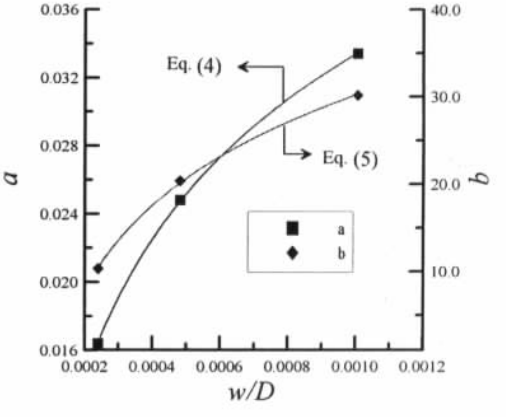

Fig.7 a and b values with the perimeter at nozzle throat

Figure 8 shows the resulting empirical lines for prediction of the discharge coefficient of the critical nozzle with rod. It is obvious that for the critical nozzle with rod, Eq.(3) using the perimeter concept can predict the discharge coefficient well.

In order to investigate the viscous effects of the critical nozzle with and without rod, Fig. 9 shows the computed kinematic viscosity profiles at the nozzle

throat, where y is the vertical distance from the rod surface, and ν is the kinematic viscosity. For Re = *87850*, the kinematic viscosity near the rod surface is lower than that near the nozzle wall. This is attributed to the local flow acceleration at the nozzle wall curvature. From these profiles it is found that the viscous effects considerably increase as D_{eq} decreases, and that an increase in Reynolds number reduces the kinematic viscosity at the nozzle throat.

Boundary layer integral properties can be obtained from the computed velocity profiles at the nozzle throat. Figures 10 and 11 present the boundary layer displacement thickness δ^* and momentum thickness θ at the nozzle throat as a function of Reynolds number. It is noted that for the critical nozzle with rod, δ^* and θ are calculated as summations of the boundary layers developed at both the nozzle wall and rod surface, while those of the critical nozzle without rod are given by only the boundary layer at the nozzle wall.

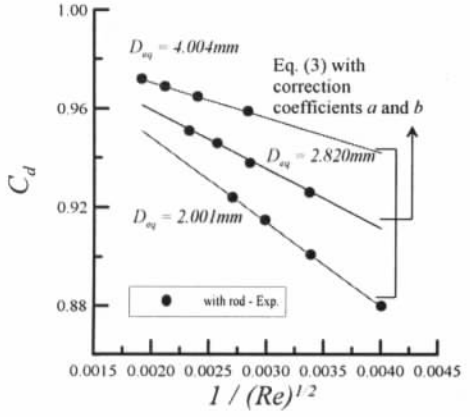

Fig.8 Corrected discharge coefficient for the critical nozzle with rod

The displacement thickness of the critical nozzle with rod significantly increases, as D_{eq} and Reynolds number decrease, as also known in the computed kinematic viscosity profiles in Fig. 9. It seems that the displacement thickness is given by a linear function of Reynolds number.

The present study is the first to investigate the variable critical nozzle flow. Both experimental and computational results indicate the usefulness of the variable critical nozzle for a wide range of mass flow rate measurements.

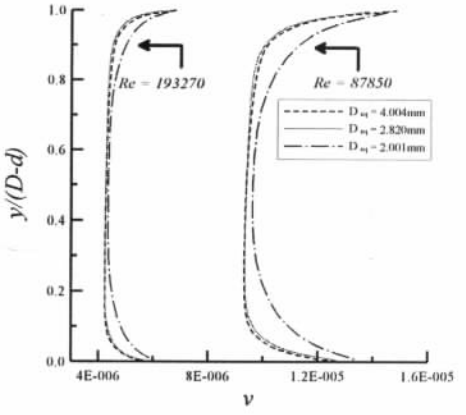

Fig.9 Predcited kinematic viscosity profiles at throat of nozzle with rod

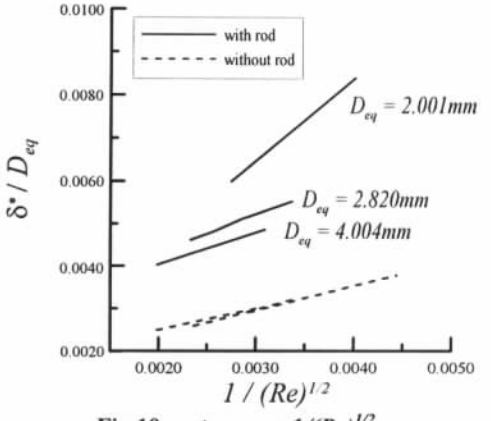

Fig.10 δ^* / D_{eq} **vs** $1/(Re)^{1/2}$

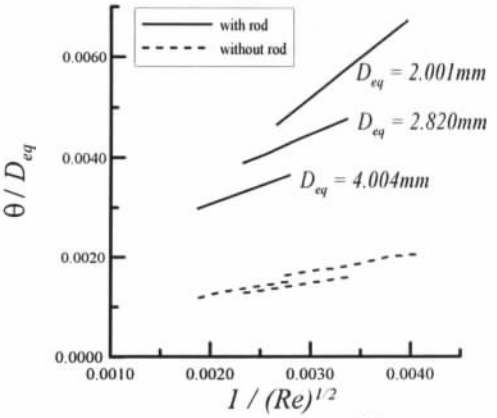

Fig.11 θ / D_{eq} **vs** $1/(Re)^{1/2}$

4. Conclusion

The present study describes experimental and computational works to investigate the effectiveness of a variable critical nozzle.

The results obtained are summarized as follow;

1. The present computations predict well the experimental discharge coefficient at high Reynolds numbers, but the predictions become somewhat poor

at low Reynolds numbers.

2. The discharge coefficient of the critical nozzle with rod is given as a function of the Reynolds number, and it increases as the equivalent diameter of critical nozzle throat and Reynolds number increase.

3. The discharge coefficient of the critical nozzle with rod can be successfully predicted by the present empirical equations involving the perimeter at nozzle throat.

4. The present results show the usefulness of the variable critical nozzle using a rod. For accurate measurement of mass flow rate, the rod diameter should make the equivalent diameter at nozzle throat as large as possible, at the range of mass flow rate measurement required.

Reference

[1] ISO9300, Measurement of Gas Flow by Means of Critical Flow Venturi Nozzles, 1990.

[2] H. W. Liepmann and A. Roshko, Elements of Gas dynamics. *John Wiley & Sons,Chapter 2*, 1957.

[3] M. Ishbashi and M. Takamoto, Theoretical Discharge Coefficient of a Critical Circular-Arc Nozzle with Laminar Boundary Layer and Its Verification by Measurements using Super-Accurate Nozzles. *J. flow Measurement and Instrumentation,* 2000, 11: 305-313.

[4] H. E. Hillbrath, The Critical Flow Venturi an Update, Flow: Its Measurement and Control in Science and Industry. *J. Instrument Society of America*, 1981, 2, pp: 407-420.

[5] J. H. Kim, H. D. Kim, S. Matsuo and T. Setoguchi, Study for the Gas Flow through a Critical Nozzle. *J. Thermal Science*, 2003, 12(3): 250-259.

[6] S. P. Tang and J. B. Fenn, Experimental Determination of the Discharge Coefficients for Critical Flow through an Axisymmetric Nozzle, *AIAA J.*, 1978, 16(1): 41~46.

[7] H. D. Kim, J. H. Kim, K. A. Park, T. Setoguchi and S. Matsuo, Study of the Unsteady Effects on the Gas Flow through a Critical Nozzle. *IMechE J. Mechanical Engineering Science*, 2003. (in press)

[8] E. von Lavante, A. Zachcizl, B. Nath and H. Dietrich, Numerical and Experimental Investigation of Unsteady Effects in Critical Venturi Nozzles. *J. Measurement*, 2002, 11: 257-264.

[9] K. A. Park, Y. M. Choi, T. S. Cha and B. H. Yoon, Evaluation of Critical Pressure Ratio of Sonic Nozzles at Low Reynolds Number. *J. Flow Measurement and Instrumentation*, 2001, 12: 37-41.

[10] Y. M. Choi, K. A. Park, J. T. Park, H. M. Choi and S. O. Park, Interference Effects of Three Sonic Nozzles of Different Throat Diameters in the Same Meter Tube. *J. Flow Measurement and Instrumentation*, 1999, 10: 175-181.

[11] N. Bignell, The Use of Small Sonic Nozzles at Low Reynolds Numbers, *J. Flow Measurement and Instrumentation*, 1996, 7: 109-114.

[12] S. Nakao, Y. Yokoi and M. Takamoto, Development of a Calibration Facility for Small Mass Flow Rates of Gas and the Uncertainty of a Sonic Venturi Transfer Standard. *J. Flow Measurement and Instrumentation*, 1996, 7: 77-83.

[13] K. A. Park, and J. S. Paik, Uncertainty of the Primary Calibration of Critical Sonic Nozzles, Devices for Flow Measurement and Control. *The American Society of Mechanical Engineers*, 1993, FED-Vol. 159: 33-40.

[14] H. D. Kim, J. H. Kim, K. A. Park, T. Setoguchi and S. Matsuo, Computational Study of the Gas Flow through a Critical Nozzle. *IMechE J. Mechanical Engineering Science,* 2003, 217: 1179-1189.

[15] K. Matsuo, Y. Miyazato and H. D. Kim, Shock Train Pseudo-Shock Phenomena in Internal Gas Flows. *Progress in Aerospace Sciences*, 1999, 35: 33-100.

[16] K. Matsuo and H. D. Kim, Post-Shock Expansion Phenomenon Caused by Normal Shock/Turbulent Boundary Layer Interaction. *J. JSME International, Series B*, 1993, 36(4): 54-62